Coercivity mechanism in $Nd_{60}Fe_{30}Al_{10}$ and $Nd_{60}Fe_{20}Co_{10}Al_{10}$ alloys

R. Sato Turtelli,[1,*] D. Triyono,[1] R. Grössinger,[1] H. Michor,[1] J. H. Espina,[2] J. P. Sinnecker,[3] H. Sassik,[1] J. Eckert,[4] G. Kumar,[4] Z. G. Sun,[4] and G. J. Fan[5]

[1]*Inst. f. Festkörperphysik, Techn. Univ. Wien, Wiedner Hauptstrasse 8-10, A1040, Vienna, Austria*

[2]*IMRE. Facultad de Física, Universidad de la Habana, San Lázaro y L. Vedado, C. Habana, CP 10400, Cuba*

[3]*Inst. de Física, Universidade Federal do Rio de Janeiro, CP 68528, 21945-970-Rio de Janeiro, Brazil*

[4]*IFW Dresden, Inst. f. Metallische Werkstoffe, Postfach 27 00 16, D-01171 Dresden, Germany*

[5]*Universität Ulm, Abt. Werkstoffe der Electrotechnik, Albert-Einstein-Allee 47, D-89081 Ulm, Germany*

(Received 31 January 2002; revised manuscript received 11 June 2002; published 29 August 2002)

The temperature dependence of the hysteresis loops and susceptibility for the melt-spun ribbon and bulk $Nd_{60}Fe_{30}Al_{10}$ and $Nd_{60}Fe_{20}Co_{10}Al_{10}$ alloys were studied. The investigations were performed on as-cast and annealed samples. Measurements of the hysteresis loops with maximum field of $\mu_0 H_{max}=22$ T were made between 4.2 and 300 K. The temperature dependence of the coercivity follows a law that describes hard magnetic behavior based on pinning-site inhomogeneities interacting with domain walls. A quantitative evaluation of the domain-wall width, the exchange and anisotropy constants was made. The coercivity of the alloys at room temperature depends strongly on the quenching rate and/or on the production method. The room-temperature coercivity of the alloys shows an exponential behavior with the Curie temperature. Depending on the quenching rate, the melt-spun Nd-Fe, Co-Al alloys form distinctly different nonequilibrium phases, indicating that the magnetically hard precursor may vary mainly with quenching rate.

DOI: 10.1103/PhysRevB.66.054441 PACS number(s): 75.60.Ej, 75.60.Nt

I. INTRODUCTION

The preparation of hard magnetic amorphous rare-earth-transition metal alloys and the study of their magnetic properties have provided the greatest stimulus for research of permanent magnets. A number of recent studies[1–8] have demonstrated that Nd-(Fe,Co)-(Al,Si) bulk (with a maximum thickness of 15 mm) amorphous alloys can be produced in the as-cast state exhibiting hard magnetic properties, developing a coercive field $\mu_0 H_c$ up to 0.38 T, at room temperature. With annealing, no significant change of the magnetic properties is observed and the hardness disappears when the materials are completely crystallized. However in Nd-(Fe,Co)-Al amorphous alloys, H_c strongly depends on the quenching rate (QR). H_c decreases with increasing of QR.[5,6]

Recent work performed by the present authors, published elsewhere,[9] reports about a coercive field of 0.039 T in a $Nd_{60}Fe_{30}Al_{10}$ ribbon with a thickness of 30 μm. Additionally, the TEM examination revealed that the nominally amorphous as-spun microstructure (x-ray diffraction spectrum is typical of an amorphous material) consists of an amorphous Nd-rich matrix with grains smaller than 10 nm of Nd crystallites (cubic, space group $Fm\bar{3}m$). In the samples annealed at 603 K for 10 min, the grain size is increased and additionally, new crystalline phases [of the compositions $Nd(Fe_{1-x}Al_x)_2$] are formed. After annealing at 773 K for 10 min the complete crystallization occurs revealing hexagonal Nd, $NdAl_2$, and Nd_2Fe_{17} crystalline phases and, at room temperature, the alloy is paramagnetic. However, at room temperature, the change in microstructure due to annealing at 603 K did almost not affect the value of the coercive field. Recently, Kramer *et al.* suggested that as-spun $Nd_{60-2/3x}Fe_{30-1/3x}Al_{10+x}$ $(-2<x<6.5)$ microstructure consists of an amorphous Nd-rich, magnetically soft matrix with clusters of approximate 1.2 nm diameter tentatively identified as antiferromagnetic $Nd_6Fe_{13-x}Al_{1+x}$ phase.[7]

The coercive field of melt-spun $Nd_{60}Fe_{30}Al_{10}$ increases up to about 4 T when the temperature decreases from Curie temperature to around 77 K and decreases quickly for temperatures lower than this temperature. The reduction of H_c below 77 K is caused by the presence of an ordered magnetic Nd and Nd-rich phases.[6,9] Wang *et al.*[6] attributed the low coercivity found in rapidly quenched $Nd_{60}Fe_{30}Al_{10}$ ribbons, at room temperature, to the presence of nonmagnetic Nd and nonuniformity of the magnetic microstructure formed by the amorphous phase and other unidentified magnetic phases. However, in our previous work, we have suggested that this can be related to the fact that the material is close to the magnetic ordering temperature.[9]

To explain the hard magnetic behavior of Nd-based bulk amorphous alloys, magnetic exchange coupling interaction between metastable magnetic ordered clusters with large random anisotropy,[1–6] or the pinning of domain walls[8,9] has been suggested. Recently, Wei *et al.*[10] have observed a large-scale magnetic domains in $Nd_{60}Fe_{20}Co_{10}Al_{10}$ bulk by using magnetic-force microscopy (average length scale of 360 nm for the as-cast sample and 420 nm for the sample annealed at 715 K for 1800 s). The existence of the large-scale domains is interpreted as a result of short-range ordering of atomic clusters in the material by exchange coupling. However to explain the invariance of the coercivity with a heat treatment, prior to full crystallization, in addition exchange coupling between ordered clusters, Wei *et al.* take also into account the pinning of domain walls.

Our point of view, the mechanism of the coercivity in melt-spun Nd-Fe, Co-Al alloys is not clear until now. Therefore, in this work, we extend the investigation of the temperature dependence of the hysteresis loops and susceptibility for the melt-spun ribbon and bulk $Nd_{60}Fe_{30}Al_{10}$ and

$Nd_{60}Fe_{20}Co_{10}Al_{10}$ alloys. Measurements of the hysteresis loops with maximum field of $\mu_0 H_{max}=22$ T were performed between 4.2 and 300 K.

II. EXPERIMENTAL

A $Nd_{60}Fe_{20}Co_{10}Al_{10}$ bulk cylindrical sample of 3 mm diameter and 50 mm length was prepared by die casting into a copper mould under argon atmosphere starting from prealloyed ingots. The structure of as-cast sample was characterized by optical microscopy, x-ray diffraction, and differential scanning calorimeter. Details of the preparation and the microstructure analysis of this sample are given elsewhere.[2] $Nd_{60}Fe_{30}Al_{10}$ and $Nd_{60}Fe_{20}Co_{10}Al_{10}$ ribbons (thickness 30 μm and width 2 mm) were prepared by melt-spinning in protective atmosphere. X-ray diffraction and electron microscopy (TEM) were used to study the microstructure at room temperature. The microstructure characterizations of $Nd_{60}Fe_{30}Al_{10}$ as-cast and annealed samples performed by TEM method are described elsewhere.[9] The Curie temperature T_C, was determined from the temperature dependence of the initial ac-susceptibility χ_i, where $d'\chi_i/dT$ shows a minimum. The initial susceptibility measurements were carried out in an ac-magnetic field of 200 A/m with a frequency of 80 Hz between 4.2 and 300 K and for higher temperatures, in a field of 100 A/m with 800 Hz. Hysteresis loops were measured between 4.2 and 300 K using a pulsed-field magnetometer with a maximum applied field $\mu_0 H_{max}$ up to 22 T (maximum rate$=$5750 T/s). Additionally, at room temperature, static hysteresis loops of all samples were measured using an extraction magnetometer Quantum Design PPMS, with a maximum external field of 8.5 T. The investigations were performed on as-cast and annealed samples. The annealing was carried out in $Nd_{60}Fe_{30}Al_{10}$ at 603 K for 10 min and in bulk $Nd_{60}Fe_{20}Co_{10}Al_{10}$, at 773 K for also 10 min.

III. EXPERIMENTAL RESULTS

The x-ray diffraction patterns of ribbons and bulk materials in the as-cast state are always indicative for an amorphous structure. The EDX measurements at several layers of $Nd_{60}Fe_{30}Al_{10}$ ribbon showed that the sample is very homogeneous with average composition of $Nd_{62}Fe_{32}Al_{3.4}Si_{2.6}$. The presence of Si atoms is due to the alloy being fused in a quartz crucible. Figures 1(a) and 1(b) show the x-ray diffraction spectra of as-cast and annealed ribbons of $Nd_{60}Fe_{30}Al_{10}$ and $Nd_{60}Fe_{20}Co_{10}Al_{10}$, respectively. No crystalline diffraction peaks are visible for the as-cast samples. However, from the TEM investigations, as reported in our previous work,[9] a precipitation of small crystallites of cubic Nd of a grain size$\leqslant$10 nm are always present. For the alloys annealed at 603 K, a mixture of amorphous and crystalline Nd-rich phases are more obvious indicated by well defined peaks together with the amorphous hump. In this sample the grain size becomes larger than 10 nm. The samples heat treated at 773 K, are completely crystallized exhibiting Nd particles with cubic and hexagonal structures, Nd_2Fe_{17} and $Nd(Fe_{1-x}Al_x)_2$ phases.[5–9]

The temperature dependencies of the initial susceptibility,

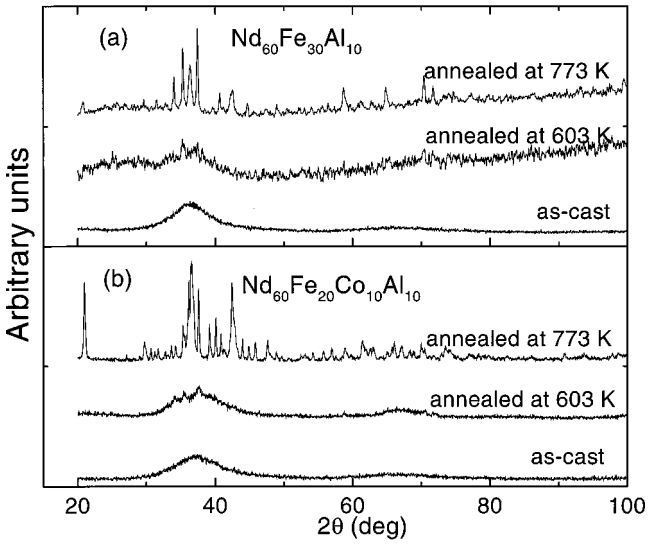

FIG. 1. X-ray diffraction spectra obtained on $Nd_{60}Fe_{30}Al_{10}$ and $Nd_{60}Fe_{20}Co_{10}Al_{10}$ ribbons.

$\chi_i(T)$, measured on as-cast and annealed samples of $Nd_{60}Fe_{30}Al_{10}$ are shown in Fig. 2. The measurements performed on ribbon and bulk $Nd_{60}Fe_{20}Co_{10}Al_{10}$ samples are presented in Fig. 3. The insets of Figs. 2 and 3 show $\chi_i(T)$ in enlarged scales at low temperatures. As can be seen, for all samples, the $\chi_i(T)$ curves present peaks close to the magnetic ordering temperatures of the Nd phase, evidencing then, the existence of the Nd-rich crystallites embedded in the amorphous matrix. These results agree with TEM investigations. Nd has a double hexagonal crystal (dhcp) structure, with two inequivalent lattice sites of approximately cubic and hexagonal symmetries. The magnetic order in Nd is multi-**q** at low temperatures. The fcc allotrope of Nd is ferromagnetic with a T_C of 29 K.[11] Neutron-diffraction measurements have shown two antiferromagnetic ordering temperatures, one at 19.9 K (the onset of ordering on hexagonal sites) and the other at 7.5 K (the onset of ordering on the

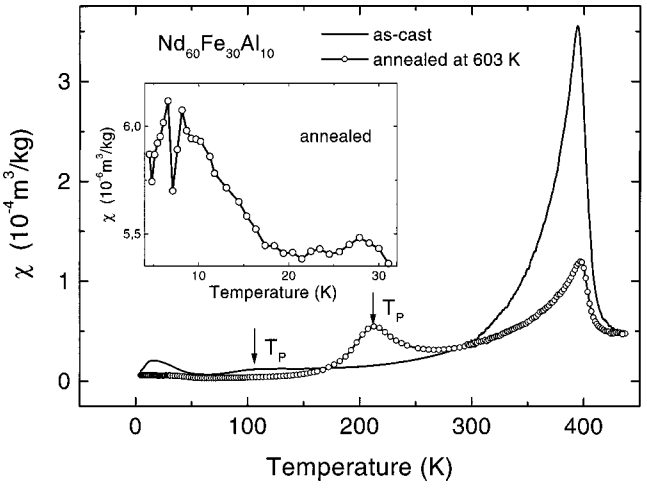

FIG. 2. Temperature dependence of the susceptibility of $Nd_{60}Fe_{30}Al_{10}$ ribbons. In inset shows the enlarged scale at low temperatures for the annealed sample at 603 K for 10 min.

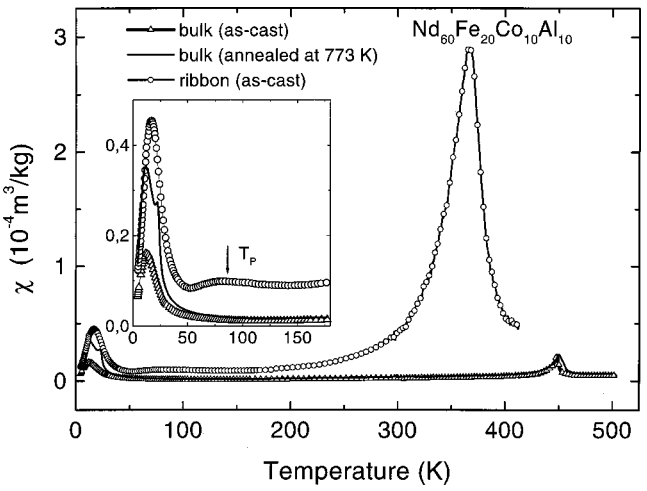

FIG. 3. Temperature dependence of the susceptibility of $Nd_{60}Fe_{20}Co_{10}Al_{10}$ samples. In inset shows the enlarged scale at low temperatures.

cubic sites), but electrical resistivity measurements have shown changes in slope at 6, 8, and 18 K.[11] In this work, susceptibility measurements showed similar results like those of resistivity measurements for the annealed ribbon $Nd_{60}Fe_{30}Al_{10}$ (see the inset in Fig. 2) showing peaks at 6.5, 8, and 28 K, then $\chi_i(T)$ decreases gradually up to 75 K. For as-cast $Nd_{60}Fe_{30}Al_{10}$ and $Nd_{60}Fe_{20}Co_{10}Al_{10}$ ribbons, a broad peak occurs at 16.5 K, while for the bulk samples, a hump at 11.3 K was found, then $\chi(T)$ decreases slowly up to 50 K. The broad magnetic transitions indicate the formation of different magnetic phases and many inequivalent local surrounding.

It is worth mentioning that the $\chi_i(T)$ measurements show an additional peak at T_P (see Figs. 2 and 3) above 75 K and before the Curie temperature (T_C) of the amorphous matrix, but only for the ribbons. This peak moves to higher temperatures when the sample is heat treated. In a previous work,[9] we had already mentioned that the appearance of this peak can be related to the nonuniformity of quenching rates along the ribbons forming distinctly different nonequilibrium phases with different microstructures or compositions. Both effects originate different magnetic ordering temperatures.[12–14] As will be reported later, they are identified as a metastable ferromagnetic Fe-Al phase. This metastable phase was not observed in the bulk material, which indicates more uniformity of quenching rate (QR) in whole sample.

Curie temperatures of the amorphous matrix T_C obtained from the minimum of $d'\chi_i/dT$ are shown in Table I. The Curie temperature of the ribbon is much smaller than that of the bulk samples and T_C increases slightly with heat treatment. The increase of T_C with an annealing can arise from the structural relaxation and the decrease of the Nd content in the amorphous matrix. On the other hand, the magnetic ordering temperature of the ribbon being smaller than that of the bulk can be related to the different quenching rates, where QR (ribbon)$\gg$QR (bulk). Croat[13,15] has reported that magnetic properties (such as coercivity and Curie temperature) of melt-spun $Nd_{1-x}Fe_x$ alloys change strongly with quenching rates and also with production method of the

TABLE I. Values of the coercivity (measured by means of a PPMS) and the Curie temperature obtained for Nd-Fe, Co-Al alloys.

Sample			$\mu_0 H_c$ (T)	T_C (K)
$Nd_{60}Fe_{30}Al_{10}$	ribbon	as-cast	0.038	401
$Nd_{60}Fe_{30}Al_{10}$	ribbon	annealed at 603 K	0.035	404
$Nd_{60}Fe_{20}Co_{10}Al_{10}$	ribbon	as-cast	0.0083	375
$Nd_{60}Fe_{20}Co_{10}Al_{10}$	bulk	as-cast	0.33	448
$Nd_{60}Fe_{20}Co_{10}Al_{10}$	bulk	annealed at 773 K	0.34	450

amorphous materials. In the Ref. 13, Croat showed that Curie temperatures of amorphous $Nd_{1-x}Fe_x$ alloys with $0.4 < x < 0.8$ are much smaller in evaporated film than those of melt-spun ribbon. For example, in $Nd_{60}Fe_{40}$, the Curie temperature is ~270 K for the film and ~480 K for the melt-spinning ribbon. Therefore, in this work, because QR (ribbon)$\gg$QR (bulk), we have attributed to the low T_C of the ribbon due to the high quenching rate.

Figures 4(a) and 4(b) show the upper part of hysteresis loops measured in a pulsed field at various temperatures on as-cast and annealed $Nd_{60}Fe_{30}Al_{10}$ samples. Magnetization curves of $Nd_{60}Fe_{20}Co_{10}Al_{10}$ ribbon and of as-cast bulk $Nd_{60}Fe_{20}Co_{10}Al_{10}$ are shown in Figs. 5(a) and 5(b), respectively. For all samples, when a maximum field of 22 T is applied, the saturated state of the magnetization was not reached due to the noncollinear sperimagnetic structure in these materials.[12,13] However, the maximum coercive field, namely, the coercivity, is obtained.

Our data show that the hysteresis loops of the bulk

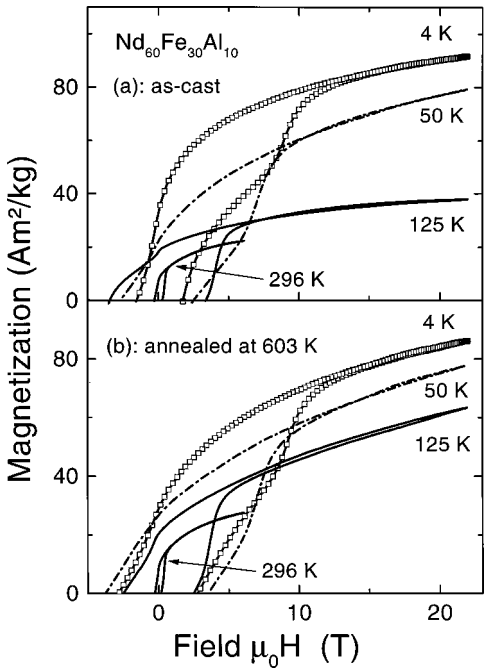

FIG. 4. Hystereis loops of $Nd_{60}Fe_{30}Al_{10}$ ribbons measured at different temperatures: (a) as-cast sample and (b) annealed sample.

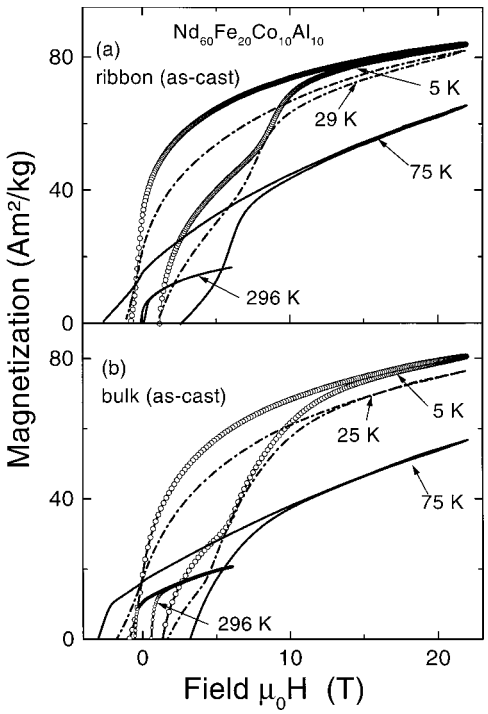

FIG. 5. Hysteresis loops of $Nd_{60}Fe_{20}Co_{10}Al_{10}$ samples measured at different temperatures: (a) as-cast ribbon and (b) as-cast bulk.

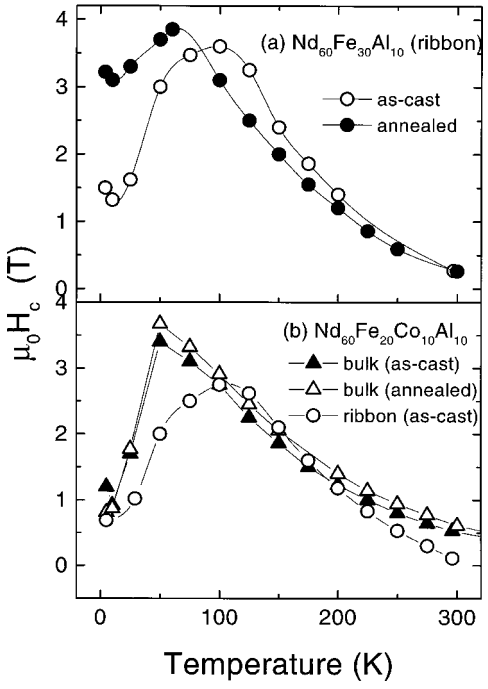

FIG. 6. Temperature dependence of the coercivity obtained on: (a) $Nd_{60}Fe_{30}Al_{10}$ samples and (b) $Nd_{60}Fe_{20}Co_{10}Al_{10}$ samples.

$Nd_{60}Fe_{20}Co_{10}Al_{10}$ measured above $T>50$ K are rectangular, while below 50 K, the loops are typical of supposing two phases. However, the hysteresis loops of ribbons (as-cast and annealed) show a kink at $H=0$ for temperatures below room temperature. Below T_P, it is clear that the metastable ferromagnetic Fe-Al phase can cause a kink close to the origin, but this kink exists also for $T>T_P$. Nevertheless the soft ferromagnetic phase really responsible for the kink could not be identified. As in the bulk, for $T<50$ K the influence of magnetically ordered Nd-rich phase appears on the hysteresis loops of ribbons.

The temperature dependencies of the coercivity of $Nd_{60}Fe_{30}Al_{10}$ and $Nd_{60}Fe_{20}Co_{10}Al_{10}$ are shown in Figs. 6(a) and 6(b), respectively. It is worth to mention that these alloys exhibit a time dependence of the magnetization, therefore the coercive field measured in pulsed fields is larger than that measured with static fields.[16]

When the temperature decreases, the coercivity increases showing a maximum at temperature T_{max} around 50, 75, and 100 K for the bulk, annealed ribbon and as-cast ribbon, respectively, then decreases up to 7.5 K and increases again. The temperature where the maximum occurs is related to the precursor from distinctly different magnetic phases were formed depending on the quenching rate used to prepare the alloy. For the bulk, the magnetic transition at low temperatures takes place rather gradual up to 50 K. In the as-cast ribbon, the maximum happens at T_P where the magnetic transition of the metastable Fe-Al occurs reducing H_c, afterwards stronger reduction of the coercivity is followed by subsequent magnetic ordering of the precipitated particles. For the annealed ribbon, the reduction of the coercivity due to the magnetic ordering of the metastable phase starts to occur at T_P much higher (~210 K). Therefore the maximum occurs at ordering temperature of the Nd-rich particles. The temperature $T_{max}=75$ K confers the Curie temperature of $NdAl_2$.[9] This phase can be present in ribbons investigated here, because the initial conditions for the formation of $NdAl_2$ are favorable due to the melting point of Al is the lowest of the other constituents. Therefore as the temperature is raised molten Al surrounds solid Nd, Fe, and Co. Since diffusion in the liquid is much more rapid than diffusion in the solid, the phases formed between Nd and Al approach from the Al-rich side during the melting process, thus the initial conditions are favorable for the formation of $NdAl_2$. The increase of H_c observed at 7.5 K can be related to the change of the ordering from the hexagonal site to the cubic site of Nd.

At room temperature, the coercivity of the ribbons is much smaller than those of the bulk samples and, the coercivity of the $Nd_{60}Fe_{30}Al_{10}$ ribbon is much larger than that of $Nd_{60}Fe_{20}Co_{10}Al_{10}$ ribbon (see Table I). These results may be related to the samples exhibiting different QR's. Croat has found in melt-spun Nd-Fe alloys, the almost linear increase in coercivity with decreasing QR. Croat has suggested that the dependence of the coercivity on quenching rate can be related to the formation of some type of semicrystalline structure in which the degree of disorder and associated anisotropy varies with quenching rate.[15] On the other hand, a degree of disorder (a degree of orientations of Fe moments with nearly randomly oriented Nd moments results in a molecular field direction at Nd sites) may also explain the strong influence of the preparation conditions on the Curie temperature. The Curie temperature of the ribbon is close to room temperature. Therefore, we ascribe the low room-temperature coercivity to the low Curie temperature. As can

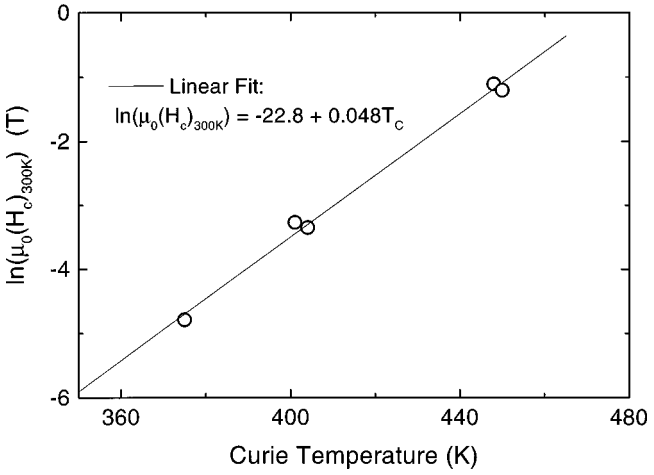

FIG. 7. Logarithm of the coercivity of different samples as function of the Curie temperature.

be seen in Table I, T_C can vary from 375 to 450 K. Consequently, it is expected that the room-temperature coercivity is dependent of the Curie temperature of the alloy. In fact, the room-temperature coercivity increases exponentially with the Curie temperature following the exponential law found by fitting $\mu_0(H_c)_{300\,\mathrm{K}}=Ce^{0.048T_C}$ to the experimental data, where $C=1.25\times10^{-10}$. The room-temperature coercivity (measured with static field, see Table I) as function of the Curie temperature is shown in Fig. 7. This exponential law is not valid for lower temperatures, on the contrary, as can be seen in Fig. 6(b), at temperatures close to the maximum of the coercivity of the ribbon, the coercivity of the bulk can become smaller than that of the ribbon.

Up to now, as mentioned before, in the most of previous works have been suggested that the origin of the high coercivity in the bulk material is due to the magnetic-exchange interaction among nanosize clusters with different local composition and magnetic properties, which hardness is related with the concentration of these clusters. A part from Kramer *et al.*,[7] the coercivity mechanism was described by the coupling between soft ferromagnetic and antiferromagnetic phases, when the later phase becomes magnetically ordered at $T_N<T_C$. They obtained a measurable hysteric behavior only below half of the Curie temperature of the soft amorphous matrix ($0.5\,T_C$). However, in our work, we suggest the strong pinning of domain walls model for explaining the coercivity mechanism of the alloys investigated here. In this case, the coercivity is the critical field required to release the wall from the pinning sites.

The initial magnetization of the hysteresis loops of the $Nd_{60}Fe_{20}Co_{10}Al_{10}$ bulk material shows a pinning-type behavior. The shape of the virgin curves of the ribbons reveals an inhomogeneous magnetization behavior in the samples. Figures 8(a) and 8(b) show the virgin magnetization curves measured on the as-cast $Nd_{60}Fe_{30}Al_{10}$ and as-cast bulk $Nd_{60}Fe_{20}Co_{10}Al_{10}$ samples. Similar curves were obtained for the annealed samples. Then, the high coercivity can arise from impediments to domain wall motion, caused by grains boundaries, surfaces, or magnetic inhomogeneities.

In Fig. 9, $(\mu_0H_c)^{1/2}$ is plotted against $T^{2/3}$ for the bulk

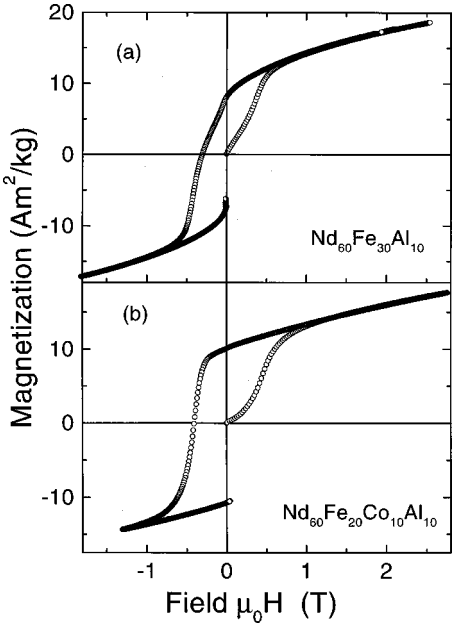

FIG. 8. Virgin curves of the magnetization measured on the as-cast samples of (a) $Nd_{60}Fe_{30}Al_{10}$ and (b) $Nd_{60}Fe_{20}Co_{10}Al_{10}$.

$Nd_{60}Fe_{20}Co_{10}Al_{10}$ magnets. The graphs are perfectly linear in the region of the temperatures $T_{\max}<T<300$ K. Similar results were also obtained for as-cast ribbons. The linear behavior between $(\mu_0H_c)^{1/2}$ and $T^{2/3}$ confers on the model proposed by Gaunt[17] based on the strong pinning of the domain walls by a random array of inhomogeneities due to thermal activation effects.

IV. STRONG PINNING MODEL

In magnetic materials, the domain walls can be pinned at magnetic inhomogeneities that may be nonmagnetic precipitates or inclusions, structural defects or cavities, or any regions with different magnetic properties from the matrix.

In $Nd_{60}Fe_{30}Al_{10}$ and $Nd_{60}Fe_{20}Co_{10}Al_{10}$ amorphous alloys,

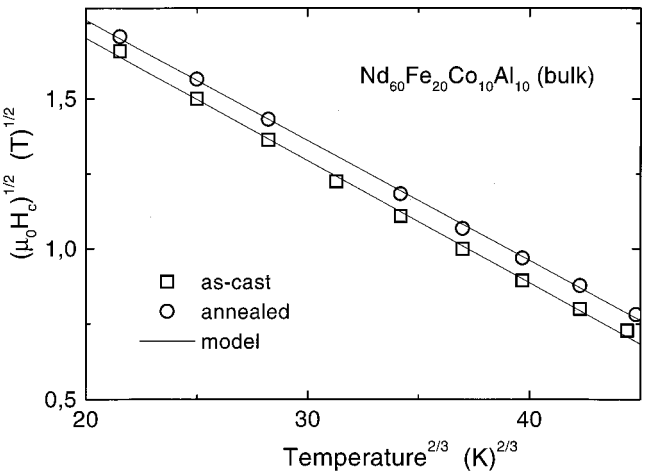

FIG. 9. $(\mu_0H_c)^{1/2}$ as a function of $(T)^{2/3}$ obtained for bulk $Nd_{60}Fe_{20}Co_{10}Al_{10}$ samples. The symbols are the experimental data and the lines are the fitting of Eq. (6) to the experimental data.

pinning sites can be attributed to the surface, structural defects and precipitation of Nd and $Nd(Fe_{1-x}Al_x)_2$ in nanocrystalline state embedded in the amorphous phase. Since these precipitation exhibit completely different magnetic properties of those of the amorphous matrix, they can act as pinning sites for domain walls of the amorphous matrix, mainly for temperatures higher than their magnetic ordering temperatures. A model of strong magnetic domain-wall pinning was developed by Gaunt considering explicitly the effect of the activation energy.[17]

On applying a field H, the wall will bow and when H increases sufficiently the wall will break away from the center pin. However, the wall can also break free in a field lower than H_0 (critical field in absence of thermal activation), if thermal energy is available to supply the activation energy which is necessary to take the bowed wall from its minimum energy position to its maximum energy position where it can break away. For strong pinning the activation energy, neglecting internal demagnetizing effects, is given by[17]

$$E=\frac{4bf}{3}\left[1-\left(\frac{H}{H_0}\right)^{1/2}\right]^{3/2}, \tag{1}$$

where f is the maximum restoring pinning force from a single pin and $4b$ is the wall width.

The condition which must be satisfied for strong domain-wall pinning is

$$\beta=\frac{3f}{8\pi b\gamma}>1, \tag{2}$$

where γ is the domain-wall energy. Thus the pinning is strong for small b (narrow domain thickness) or for large f/γ. For a 180° domain wall, the thickness and the energy are given by

$$\delta=4b=\pi\sqrt{A/K} \tag{3}$$

and

$$\gamma=4\sqrt{A.K}, \tag{4}$$

respectively, where A and K are exchange and anisotropy constants. The coercive field H_c, in the region where the intrinsic magnetic properties can be considered constant, is given by

$$\sqrt{H_c}=\sqrt{H_0}-\sqrt{H_0}\left(\frac{\ln\frac{\tau}{\tau_0}k_B}{4bf}\right)^{2/3}T^{2/3}, \tag{5}$$

where k_B is the Boltzmann constant, τ is the time duration of measurement and τ_0 is a time constant of order $10^{-7}-10^{-13}$ s.

V. EVALUATION OF MAGNETIC CONSTANTS: DOMAIN WALL, EXCHANGE AND ANISOTROPY CONSTANTS

From fitting the Eq. (5) to the experimental data and from experimentally accessible quantities which supports the validity of using the proposed model, one can estimate the magnetic constants of these materials, as domain wall energy and thickness, anisotropy and exchange constants, which are still unknown in the literature.

TABLE II. Values of the linear and angular coefficients obtained from the fitting of Eq. (6) to the experimental data of the bulk $Nd_{60}Fe_{20}Co_{10}Al_{10}$ samples.

Sample (bulk)	$\mu_0 H_0$ (T)	$(\mu_0 H_0)^{1/2}$ $(T^{1/2})$	c $(T^{1/2}\,K^{-2/3})$
$Nd_{60}Fe_{20}Co_{10}Al_{10}$ (as-cast)	6.35±0.04	2.52±0.02	0.0407±0.0007
$Nd_{60}Fe_{20}Co_{10}Al_{10}$ (annealed)	6.55±0.02	2.56±0.01	0.0400±0.0004

Equation (5) can be rewritten by

$$\sqrt{\mu_0 H_c}=\sqrt{\mu_0 H_0}-cT^{2/3}, \tag{6}$$

where

$$c=\sqrt{\mu_0 H_0}\left(k_B\ln\frac{\tau}{\tau_0}\Big/\,4bf\right)^{2/3}. \tag{7}$$

Fitting Eq. (6) to the experimental data is shown in Fig. 9. The $\sqrt{\mu_0 H_0}$ and c constants determined are listed in Table II.

The value of the domain wall thickness $\delta=4b$ can be evaluated from c estimating the maximum restoring force f per pin in the material of spontaneous magnetization M_s by means of the Néel model[18]

$$f=0.86.\frac{8}{9}(\pi Ms\rho)^2, \tag{8}$$

where the precipitates are considered as spheres with a diameter of 2ρ.

Taking into account that Eq. (5) is valid in the region of the temperatures where the intrinsic properties can be considered constant, the estimate of the magnetic properties was made for the bulk material where the magnetization at 6 T changes slightly (about 10%) in the range 100 and 350 K (see Fig. 10). Then, the average magnetization of the bulk alloy was considered to be $M_s=0.3$ T. Assuming the average diameter of pinning sites to be 10 nm the value of f results in 5.4×10^{-6} d. In this experiment, the time duration τ is approximately 3.8×10^{-3} s (the time corresponding to the field varying from the maximum field to the coercive field). Thus, assuming $\tau_0=10^{-11}$ s, a value of 7.7 nm was obtained for the domain wall width. This result shows that it is very probable that domain walls can be pinned by particles, once the condition $4b<2\rho$ is satisfied.

The anisotropy and exchange constants and domain wall energy were estimated considering 180° domain walls and the condition which must be satisfied for strong domain-wall pinning. Thus, using the Eqs. (2), (3), and (4), the following numerical results were obtained: $\gamma<3.19$ erg/cm^2, $K<3.3\times10^6$ erg/cm^3, and $A<2\times10^{-7}$ erg/cm. These results are reasonable since the hard magnetic properties of melt-spun Nd-Fe, Co-Al alloys arise from the amorphous matrix. Additionally, the value of the magnetic anisotropy constant ob-

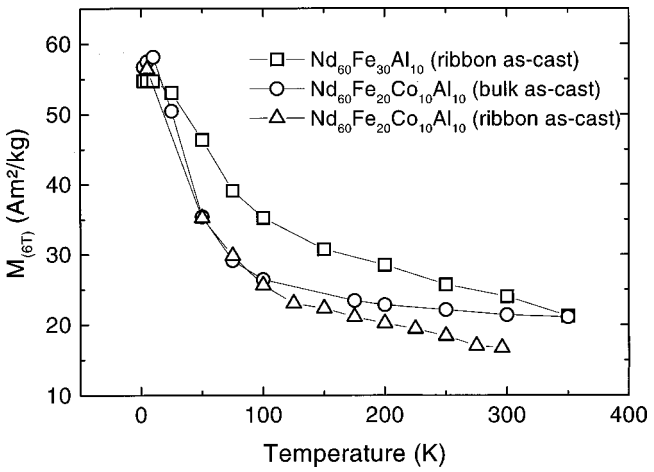

FIG. 10. Temperature dependence of the magnetization at 6 T measured on the as-cast $Nd_{60}Fe_{30}Al_{10}$ and $Nd_{60}Fe_{20}Co_{10}Al_{10}$.

tained here is comparable to the K values of amorphous Nd-Fe alloys reported by Taylor *et al.*[12] In thin film samples of amorphous $Nd_{0.3}Fe_{0.7}$, they found $K=1.7\times10^6$ erg/cm^3 for room temperature and 4.1×10^6 erg/cm^3 for 4.2 K.

VI. DISCUSSION

The observation of the proportionality between $(\mu_0 H_c)^{1/2}$ and $T^{2/3}$ in Nd-Fe Co-Al alloys demonstrates that the strong pinning model can be suggested to explain the coercive mechanism in these materials.

In our investigations, the particles precipitated in the amorphous matrix during the quenching process are paramagnetic at high temperatures and may act as pinning sites for the domain walls of the amorphous matrix. The role of particles (if they are very small) as a pinning center disappears when the particles become magnetically ordered. Consequently the number of pinning sites reduces and the magnetic particles which exhibit a small coercivity will contribute for the global magnetization curve of the alloy. Therefore an abrupt decrease of the coercivity occurs at the ordering temperature of the particles, since close to magnetic transition, the contribution due to the magnetization of the particles is negligible.

When the alloys are submitted to a heat treatment, the particles precipitated in the amorphous matrix increase in their sizes or their numbers can grow depending on the production history, then pinning of domain walls becomes stronger increasing the coercivity of the alloys. Generally speaking, when the precipitation are relatively large, the grain boundary can continue to act as pinning center even below the magnetic transition of the particles. It is clear that in our work, the increase of the coercivity with annealing is mainly due to the change of the size or number of the precipitation of particles. However for the ribbon, the high coercivity found for $T<T_{\max}$ leads to suggest at the same time the effect of the change of the composition of the remaining amorphous phase, enriching the concentration of transition metals. For the amorphous Nd_xFe_{1-x}, the coercive field is constant between $x=0.55$ and 0.4 at room temperature,[13] however at 4.2 K, the coercive field increases almost by factor 1.7 in the same range of x.[12]

In the ribbon, the proportionality between $(\mu_0 H_c)^{1/2}$ and $T^{2/3}$ is also observed in the range of the temperatures $100\ \mathrm{K}<T<300\ \mathrm{K}$. This result is due to the magnetization which varies linearly with temperature (see Fig. 10) and additional temperature dependent intrinsic magnetic effects may also vary linearly with temperature.

VII. CONCLUSION

The strong pinning model can describe the temperature dependence of the coercivity of melt-spun Nd-(Fe, Co)-Al alloys.

The coercivity of the alloys at room temperature depends strongly on the QR and/or on the production mechanism. At room temperature, the coercivity of the alloys shows an exponential behavior with the Curie temperature. Depending on quenching rate, in the melt-spun Nd-Fe, Co-Al alloys form distinctly different nonequilibrium phases. The magnetically RT-hard precursor may vary mainly with quenching rate. The abrupt decrease of the coercivity below the ordering temperature of the precipitated particles is due to these particles being magnetically softer than amorphous matrix and can lose their property to act as pinning sites.

ACKNOWLEDGMENTS

J. P. Sinnecker is grateful for the financial support of FAPERJ and CNPq. The authors wish to thank the participants of the Brazilian PRONEX/FINEP/CNPq Project No. 41.96.0907.00 for the PPMS measurements. The work was also partly supported by the Austrian National Science Foundation under the Project No. PHY 13146 and ÖAD-EZA Project No. 894/2001.

*Email address: reiko.sato@ifp.tuwien.ac.at

[1] A. Inoue, Mater. Sci. Eng. A **226–228**, 357 (1997).
[2] G. J. Fan, W. Löser, S. Roth, J. Eckert, and L. Schultz, J. Mater. Res. **15**, 1556 (2000).
[3] G. J. Fan, J. Eckert, W. Löser, S. Roth, and L. Schultz, Mater. Sci. Forum **343–346**, 97 (2000).
[4] Y. Li, J. Ding, S. C. NG, and X. Z. Wang, J. Magn. Magn. Mater. **187**, L273 (1998).
[5] X. Z. Wang, Y. Li, J. Ding, L. Si, and H. Z. Kong, J. Alloys Compd. **290**, 209 (1999).
[6] L. Wang, J. Ding, Y. Li, Y. P. Feng, X. Z. Wang, N. X. Phuc, and N. H. Dan, J. Magn. Magn. Mater. **224**, 143 (2001).
[7] M. J. Kramer, A. S. O'Connor, K. W. Dennis, R. W. McCallum, L. H. Lewis, L. D. Tung, and N. P. Duong, IEEE Trans. Magn. **37**, 2497 (2001).
[8] N. H. Dan, N. X. Phuc, N. M. Hong, J. Ding, and D. Givord, J. Magn. Magn. Mater. **226**, 1385 (2001).
[9] D. Triyono, R. Sato Turtelli, R. Grössinger, H. Michor, K. R. Pirota, M. Knobel, H. Sassik, T. Mathias, S. Höfinger, and J. Fidler, J. Magn. Magn. Mater. **242–245**, 1321 (2002).

[10] Bing Chen Wei, W. H. Wang, M. X. Pan, B. S. Han, Z. R. Zhang, and W. R. Hu, Phys. Rev. B **64**, 012406 (2001).
[11] S. Legvold, in *Ferromagnetic Materials*, edited by E. P. Wohlfarth (North-Holland, Amsterdam, 1980), Vol. 1, p. 183.
[12] R. C. Taylor, T. R. McGuire, J. D. Coey, and A. Gangulee, J. Appl. Phys. **49**, 2885 (1978).
[13] J. J. Croat, J. Magn. Magn. Mater. **244**, 125 (1981).
[14] M. Lü, M. Reissner, W. Steiner, D. S. Dai, and A. Wagendristel, J. Phys. Colloq. **C8**, 1353 (1988).
[15] J. J. Croat, J. Appl. Phys. **53**, 3161 (1982).
[16] R. Sato Turtelli, D. Triyono, R. Grössinger, M. Knobel, K. R. Pirota, J. Eckert, P. Kerschl, and S. Kato, in Proceedings of the 17th International Workshop of Rare Earth Magnets and Their Applications, Delaware, 2002 (unpublished).
[17] P. Gaunt, Philos. Mag. B **48**, 261 (1983).
[18] L. Néel, Can. J. Phys. **4**, 21 (1944).